Design of a fleet of vehicles

Gonçalo dos Santos Pereira
goncalo.s.pereira@tecnico.ulisboa.pt

Instituto Superior Técnico, Universidade de Lisboa, Portugal

February 2021

Abstract

We pre dimensioned an autonomous electric vehicle for the transportation of passengers and luggage in airports, which would travel through tunnels between the terminals and airplane. The vehicle is 5 m long and 1,8 m high and wide, with a total weight of 920 kg and a maximum mass of around 2 tons. With maximum load, the height of the center of mass of the passenger vehicle is 0,47 m above the wheel axle. The propulsion power is 4 kW and the nominal speed is 7 m s^{-1}. At nominal speed, a typical trip takes about 3.5 minutes, with a consumption of 236 Wh. 85 kg of lithium batteries are sufficient for 10 hours of continuous operation. The proposed guiding system is based on an optical system that follows a reflective tape placed on the floor. It was found that the image, captured with video cameras and digitally treated, guarantees the correct tracking and a good level of comfort at the nominal speed. The suspension has a stiffness of 20 kN / m and a damping factor of 0,2. At nominal speed, the suspension exhibits resonance peaks in the acceleration spectrum at frequencies of 1 Hz and 16 Hz, with good attenuation in the range frequency critical for human comfort. The maximum deflection of the suspension springs due to longitudinal and lateral forces is about 1 cm.

Key words: Propulsion power, energy, guiding system, suspension and comfort.

1. Introduction

In 2017 ANA *Aeroportos* launched an international contest to find a solution to a long time problem of the Lisbon airport: parking the airplanes in the remote locations, far away from the boarding area; making the passengers to take a bus from the gate to the airplane in order to board. This was time consuming and very uncomfortable to the passengers.

The best solution design by (André , *et al.*, 2017) proposed a network of dedicated underground tunnels that would directly connect the boarding gates to the parking area were the airplanes were stationed.

An electric and autonomous vehicle would then carry cargo, passengers and luggage to and from the plane to the terminals. The purpose of this thesis is to the design these vehicles taking into account different restrictions. Since the design of cargo vehicles is identical to passenger's vehicles, we only analyzed the transport of passengers.

An autonomous driving system is very complex: needs to allow driving at higher velocities, (such as 25 m s^{-1}); process images from different high resolution cameras in real time and integrate the information in less than 0,1 s; requires very high computational power that have large energy consumptions (in magnitude of the energy spent for propulsion). Thus in this thesis we want to develop a guiding system with low energy consumption, low complexity, but with good comfort and safety parameters. In our case there is no need to interpret complex images because there is not intersections with other type of traffic or obstacles; the route is known in advance and the vehicle only needs to track a reflective band on the ground. This technology is not standard and therefore is critical element of our design.

2. The Vehicle: Main dimensions and considerations

In (André , *et al.*, 2017) some main considerations regarding these vehicles were already proposed and will serve as a starting point for our analysis. The geometry

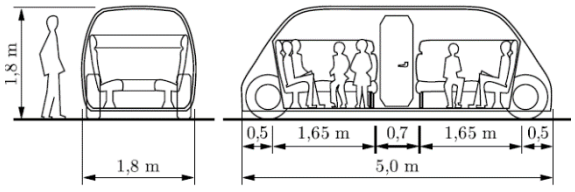

Figure 2.1: Geometry and dimensions (André , et al., 2017)

adopted is shown in figure 2.1. The vehicle carries 10 passengers and their respective luggage. The nominal velocity was fixed at 7 m s^{-1}, a compromise between reducing travelling time and reducing energy consumption, propulsion power and danger accidents probabilities (see chapter 1 (Pereira, 2020) for further analysis). This velocity allows a transport rate of around 250 passengers per minute; a higher nominal velocity would decrease the fleet productivity.

As for capacity of the vehicle, it was fixed at 10 passengers because it optimizes the fleet productivity: smaller vehicles have lower boarding times allowing for a better organization inside the plane; it's easier to sit 10 passengers every few minutes than 100 each time. In addition, a higher capacity requires larger vehicles that consume more energy, require more traction power and therefore more expensive.

3. Propulsion Power and Energy Consumption

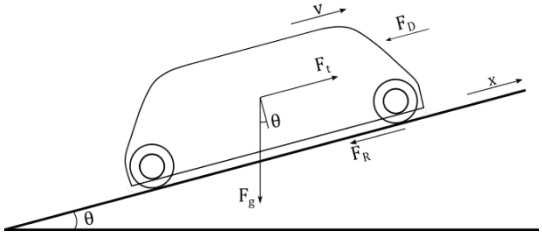

Figure 3.1: Force diagram of road with positive slope gradient.

The mains resistive forces that act upon a vehicle are rolling resistance F_R, aerodynamic drag F_D and the longitudinal component of the weight F_g. A force diagram is shown in figure 3.1 for a road with positive slop. The balance force equation is given by

$$m\frac{dv(t)}{dt} = F_t - F_D - F_R - F_g \quad (3.1)$$

Where m is total mass of the vehicle and v is its instantaneous velocity. F_t is the propulsion force given by the electric motor.

It is now important to analyze each section of a typical route taken by the vehicle to evaluate the propulsion effort, energy consumption and travelling time.
Let us first considerer a section of the path without slope. In this case, only the drag and the rolling resistance oppose the motion of the vehicle. The solution of equation 3.1 is given by

$$v(t) = v_0 - gft - \frac{\rho AC_D}{2m}\int_0^t v^2 dt + \frac{P_t}{m}\int_0^t \frac{1}{v}\,dt \quad (3.2)$$

Where f is the coefficient of rolling resistance, g is gravitational acceleration, A is the frontal section area of the vehicle, ρ is the air density, C_D is the drag coefficient and P_t is the propulsion power.

In chapter 2.2 (Pereira, 2020) it was analyzed the impact of the propulsion power for two vehicles: one with a mass of 1 ton and another with a mass of 2 ton with different constant accelerations. We concluded that 2 kW of power were enough to allow driving at constant speed of 7 m s^{-1} for both masses. If we wanted a constant acceleration of 0,25 m s^{-2}, 4 kW of power would give enough propulsion force for v < 5,5 m s^{-1}. It is important to notice that with an acceleration of 0,25 m s^{-2} the vehicle reaches nominal speed in around 98 m (28 s). Increasing the acceleration to 1 m s^{-2} would only reduce the distance to 24,5 m but it increases the power 10 times more, a significant increase for such a small reduction in the time necessary to achieve nominal speed. Furthermore, the vehicle will not enter a zero gradient section of the route from rest, but from a negative slope road where we will use its own weight to gain acceleration. At a constant speed of 7 m s^{-1} a 2 ton vehicle spends around 85 Wh to travel 1 km.

Now let us consider that the vehicle climbs a road with positive slope. This example is where the propulsion force is maximum due to the longitudinal component of the weight. The solution of equation 3.1 is given by

$$v(t) = v_0 - gt\left(i - f\sqrt{1-i^2}\right) - \frac{\rho AC_D}{2m}\int_0^t v^2 dt + \frac{P_t}{m}\int_0^t \frac{1}{v}\,dt \quad (3.3)$$

Where i = sin θ. For a constant power, the velocity reaches a minimum when the equilibrium between the resistance forces and propulsion force are reached, here denominated v_{lim}. In figures 3.2 and 3.3 we show the coefficient v_{lim}/v_0 for different values of power and slope gradient for vehicles with a mass of 1 ton and 2 ton, respectively.
This limit velocity increases with the increase of power and decrease of the slope gradient. For a mass of 1 ton, 4 kW of power make the velocity increase beyond the

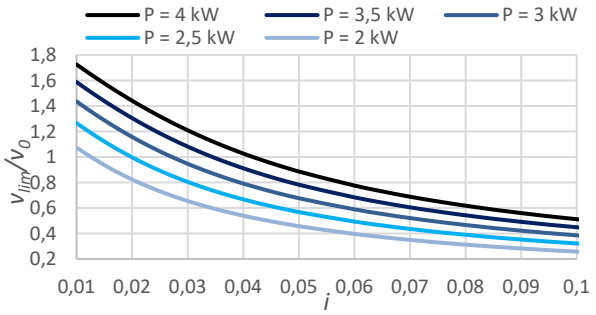

Figure 3.2: Limit velocity for m = 1 ton and v_0 = 7 m s^{-1}.

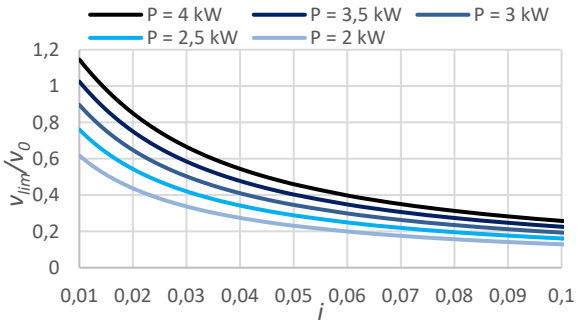

Figure 3.3: Limit velocity for m = 2 ton and v_0 = 7 m s^{-1}.

nominal velocity for a large range of slope gradients (for i < 0,04), as for the 2 ton vehicle the same happens for i < 0,015.

Usually a positive slope gradient will occur when vehicle climbs from the base of the tunnel to the first floor of terminal or to the parking lot where the airplane is stationed. Thus after a climb we want the vehicle to stop, thus increasing the traction power beyond the 4 kW has little gain. Furthermore, higher power requires motors that are more expensive that spend more energy, requiring more batteries thus increasing the weight.

However, it is import to study the impact of propulsion power on the energy consumption and travelling distance. Thus, as an example let us assume that vehicle needs climb 8 m from the base of the tunnels to the first floor of the terminal. Since we want to study the impact

of slope gradient, for fair comparison let us fix the longitudinal distance travelled at 300 m. When the slope gradient is high enough that the vehicle climbs the 8 m in less than 300 m, the rest is travelled with zero gradient. Also, we assumed that v_0 = 7 m s^{-1}.

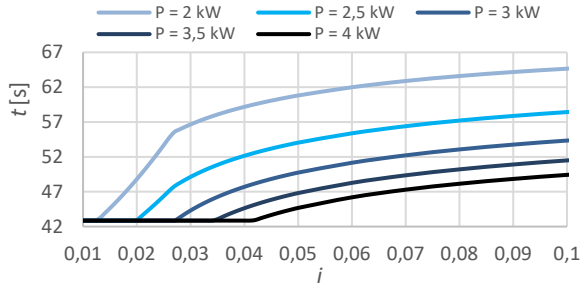

Figure 3.4: Climbing up time for m = 1000 kg, v_0 = 7 m s^{-1}

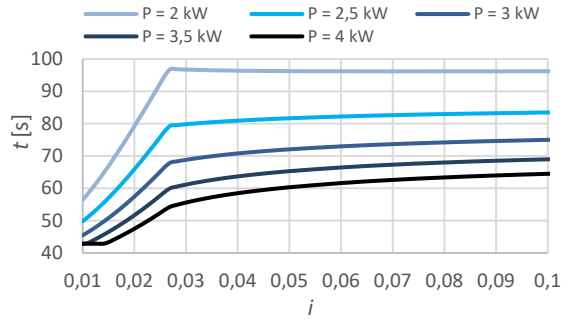

Figure 3.5: Climbing up time for m = 2000 kg, v_0 = 7 m s^{-1}

As we can see there is a significant decrease in climbing time with the increase of power. For i = 0,05, changing from 2 kW to 4 kW decreases the climbing time by 36 % and 27% for a mass of 2 ton and 1 ton, respectively. Furthermore, 4 kW of power has a large range of slope gradients were the climbing time is constant because it allows the climb to be done at nominal speed. If we did not limit the speed the vehicle would accelerate beyond 7 m s^{-1} by the ratios given in figures 3.2 e 3.3.

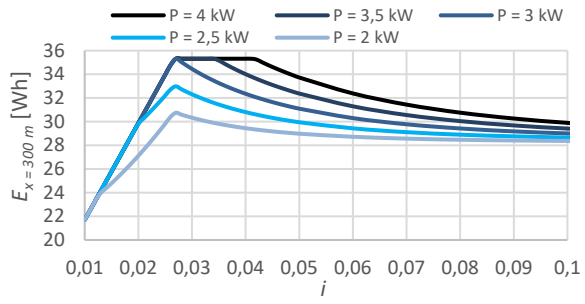

Figure 3.6: Energy consumption for m = 1000 kg, v_0 = 7 m s^{-1}

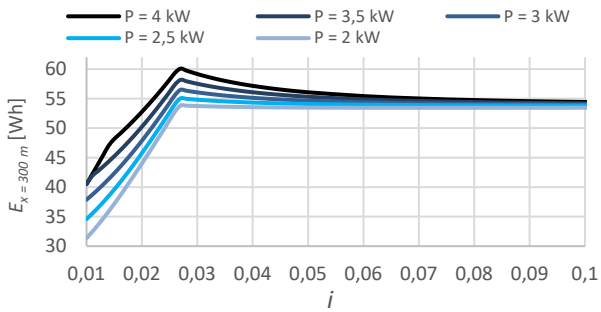

Figure 3.7: Energy consumption for m = 2000 kg, v_0 = 7 m s^{-1}

The higher the power the larger the range of slope gradient for which the energy consumption is constant because propulsion force is enough to maintain the climb speed at the nominal value of 7 m s^{-1}. For i = 0,05, changing from 2 kW to 4 kW increases the energy consumption by 16 % for a mass of 1 ton and 4 % for 2 ton, while the climb time reduces 27 % and 37 %, respectively. Therefore, increasing the power has a greater advantage for heavier vehicles since it can significantly decrease climbing time while the increase in energy consumption is less significant.

Now let us consider the opposite, a vehicle moving downhill from the first floor of the terminal to the base of the tunnels. The solution of equation 3.1 is equal to 3.3 changing the minus sine on the longitudinal component of the weight.

Usually the vehicle will star the descend from rest, so propulsion force will be limited by the friction force, that is the maximum force that can be applied without slip between the surface of the tire and the surface of the road.
The velocity below which the traction force is limited by friction is given by (see (Pereira, 2020) chapter 2.4 for details)

$$v_{\mu_k} = \frac{P_t}{\mu_k mg\sqrt{1-i^2} - mgi + < D >}$$

In (Pereira, 2020) we show that only when v < 0,5 m s^{-1} thus friction limits the traction force.
If we were to apply the maximum traction force in start of the drive, the module of variation of the acceleration $|j|$, jerk, would be high, thus it is important to constraint this parameter to allow for a better riding comfort. For good comfort |j|≤ 1 m s^{-3} and |a| ≤ 2 m s^{-2} (André, 2006).

Taking into account the restriction let us now consider the same example as we did for climbing up 8 m from the base of the tunnel to the terminal. In this case it will be the reversed, we will climb down 8 m from the terminal to the tunnel. We will also fixed the travelling distance to 300 m as before and when the slope gradient is big enough to make the climb in less than 300 m, the rest of distance will be driven with zero gradient.

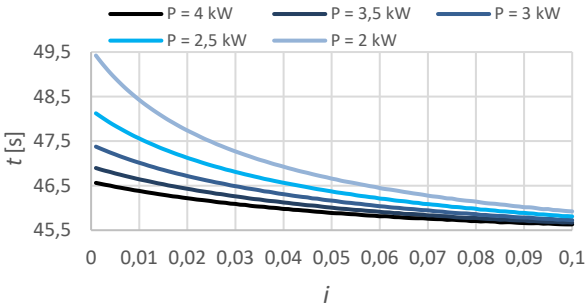

Figure 3.8: Climbing down time for m = 1000 kg, v_0 = 0 m s^{-1}

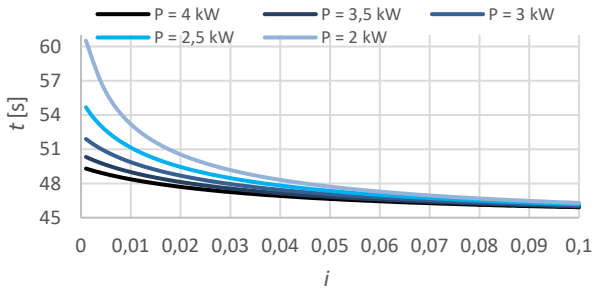

Figure 3.8: Climbing down time for m = 2000 kg, v_0 = 0 m s^{-1}

As we can see, the increase of power reduces the travelling time for small gradient slopes (i < 0,015). For i = 0,01 and a mass of 1 ton there is a reduction of 4 % when changing from 2 kW to 4kW and 12 % for a mass of 2 ton.

Once the nominal velocity is reached the vehicle brakes. The braking power can be converted in energy, E_b (for details see chapter 2.4 (Pereira, 2020)) to be stored in the batteries using regenerative braking systems. With a converting efficiency of 50 % it is possible to recover almost up to 50 % of energy spend to drive 300 m with zero gradient slope. Important to notice that for i < 0.015 it is impossible to use regenerative braking because the sum of resistance forces is higher than the longitudinal component of the weight and therefore we need to use the propulsion power to maintain the nominal speed.

After analysing the effect of the propulsion power, weight and road slip gradient on each road section that vehicle can take, it is important to analyse the whole route as one. Thus, let us assume the vehicle starts at rest in parking lot where the planes are stationed and climbs down 8 m to the base of the tunnel, then drives trough a zero gradient slope section and then climbs up 8 m to the the terminal. We will analyse the climbs with two different gradients: i = 0,05 and i = 0,1. For a fair comparison we will fix the total distance at 1,32 km for both cases. For the first example, the distance travel at zero gradient will be 1 km and in the second will be more,

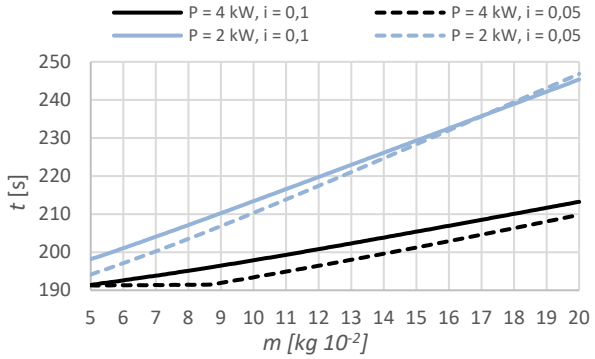

Figure 3.9: Driving time

1,16 km, to compensate for the smaller distance travel in gradient slope section due to the higher gradient. We will limit the maximum velocity to 7 m s^{-1}, the module of the acceleration to 2 m s^{-2}, the module of the jerk to 1 m s^{-3} and a regenerative braking efficiency of 80 %.

As we can observe in figure 3.9, an increase in road

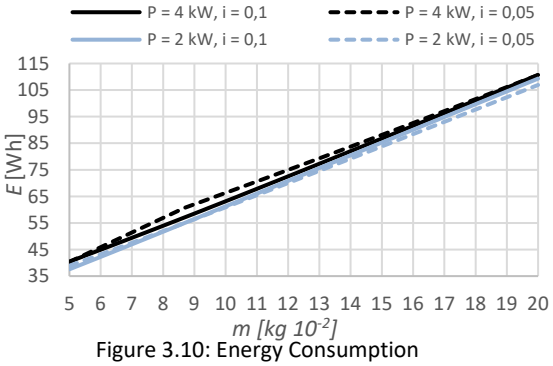

Figure 3.10: Energy Consumption

gradient leads to higher driving times for a large range of masses, mainly because the final climb up to the terminal is done with a low average speed. For P = 2 kW this happens for m < 1700 kg and for P = 4 kW happens for all the mass range depicted. The lower the slope and the greater the power the larger the mass range for which the driving time is constant, because most of route is driven at speeds very close to nominal. As for the energy consumption (figure 3.10) there is a small saving when P = 2 kW and m < 900 kg when slope is higher. For P = 4 kW that happens when m < 550 kg. This happens because the vehicle speeds up to 7 ms^{-1} faster when climbing down form the parking lot allowing regenerative braking to start earlier and thus decreasing consumption.

For P = 4 kW a 2 ton vehicle spends around 115 Wh and takes 213 s to drive the route depicted, let us assume we add an additional 30 s to embark all passengers during which the vehicle is still and charging, the total time is then 243 s. An additional 25 Wh are needed for illumination, powering up the guiding and sound systems making the total consumption reach 136 Wh per lap. In (Pereira, 2020) chapter 2.6 different type's batteries are analysed taking into account energy and power densities, charging time and price. For a continuous 10 h operation cycle the LG E-63 modules allow for the lightest system weighting around 83 kg and costing around 4 k€. As for the electric motor, OMETEC has small, lightweight motors with 1 kW to 1,5 kW with efficiencies around 85 % that cost 200 €/motor. For safety, reasons it is better to divide the traction power between the four wheels, one motor for wheel, because in case of failure of one motor the other three can safely stop the vehicle.

4. Guiding System

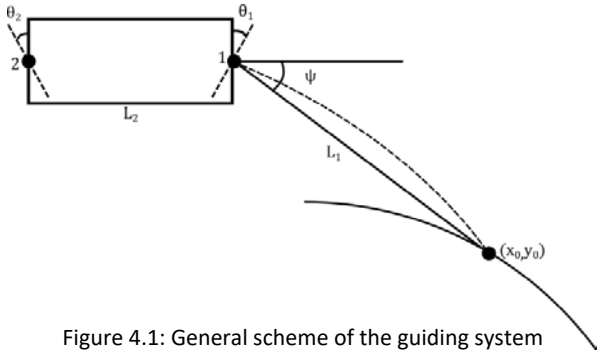

Figure 4.1: General scheme of the guiding system

The general scheme of the proposed guiding system is showed in figure 4.1. A pair of video cameras determine the target point 0 locate over the midline of the path to be driven. A reflective tape that contrast with the floor identifies this line. According to the angle ψ that the target direction makes with the vehicle's axis, an algorithm calculates the average angles θ_1 and θ_2 of the front wheel axis and the rear wheel axis. Let us compare two versions of this algorithm: one, version 1, calculating the angles θ_1 and θ_2 that drive point 1 (midpoint of the front wheels) to pass through the target point 0; another, version 2, calculating the angles θ_1 and θ_2 so that point 2 (midpoint of the rear wheels) passes through target 0. To compare the two versions of the algorithm, we analyze the system response to various types of disturbances. Furthermore, we analyze« the influence of digital filters on the vehicle's response to different input disturbances, namely the amplitude of the acceleration spectrum, in order to optimize comfort and safety.

In (Pereira, 2020) chapter 1 there is a geometric definition of the reflective tape that the vehicle needs to follow. In chapters 3.2 and 3.3 we can find the kinematic equations that describe each algorithm, is important to notice that angle θ_2 is a function of the local curve radius and is previously know, thus has feedback loop.

After defining the geometric and kinematic equations of each algorithm, it is import to discuss its response to different disturbances. One of these disturbances is optical noise of the aiming angle ψ, this happens because of the wear of the reflective band over time. These errors make the target point (point 0) oscillate over an average position over time (see figure 4.2), the disturbed angle $\widetilde{\Psi}$ is defined as $\widetilde{\Psi}(t) = \Psi(t) + \Delta\Psi(t)$ where the error is $\Delta\Psi(t) = A_0 \sin\left(\frac{2\pi v}{\lambda} t\right)$ with amplitude A_0 and wavelength λ. Thus, it is possible to define a spectral density of these disturbances as well as its derivatives.

ISO 8608 defines a set of spectral densities of vertical road irregularities for different road surfaces conditions. Usually, it is assumed that there is a similar density spectrum for the horizontal irregularities. Since it is

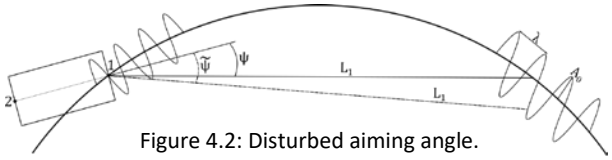

Figure 4.2: Disturbed aiming angle.

difficult to quantify the spectral density noise of the position of point zero we shall assume the same spectral function for roads of class C/D (medium condition) of ISO 8608. (See chapter 3.4 (Pereira, 2020) for further details).

In figure 4.3 we can see the acceleration spectrum of the front axle (point 1) and rear axle (point 2) for both algorithms without any mitigating measures. For any given trajectory of point 1, point 2 follows it attached by the length L_2. This type of guiding system reduces the amplitude of the disturbances of point 2 relative to point 1.

When integrating the kinematic equations (described in chapters 3.1 to 3.3 (Pereira, 2020)), we use a temporal step such that the spatial step was two orders of magnitude smaller than the wavelength of the disturbance. In addition, the amplitude of the disturbance was reduced for high frequencies, since for that frequency range the spectrum of irregularities decreases dramatically.

For short wavelengths (f> 1 Hz), algorithm 2 has a smaller transfer function amplitude than algorithm 1, the largest reduction being for the front axle. For longer wavelengths (f <0.1 Hz), the opposite is true, algorithm 2 has a greater response amplitude than algorithm 1 (chapter 3.4 (Pereira, 2020)). In particular, for long wavelengths the acceleration spectrum of algorithm 2 it's bigger (see figure 4.3)

It is beneficial for the guiding system to respond to low frequency disturbances, as they may represent a characteristic of the path to follow. It is advantageous that the vehicle responds to these disturbances to correct the trajectory without hitting the tunnel walls.
High frequency noises will be typical of small random irregularities, such as the wear of the reflective tape. It is desirable that the guiding system filters this noise in

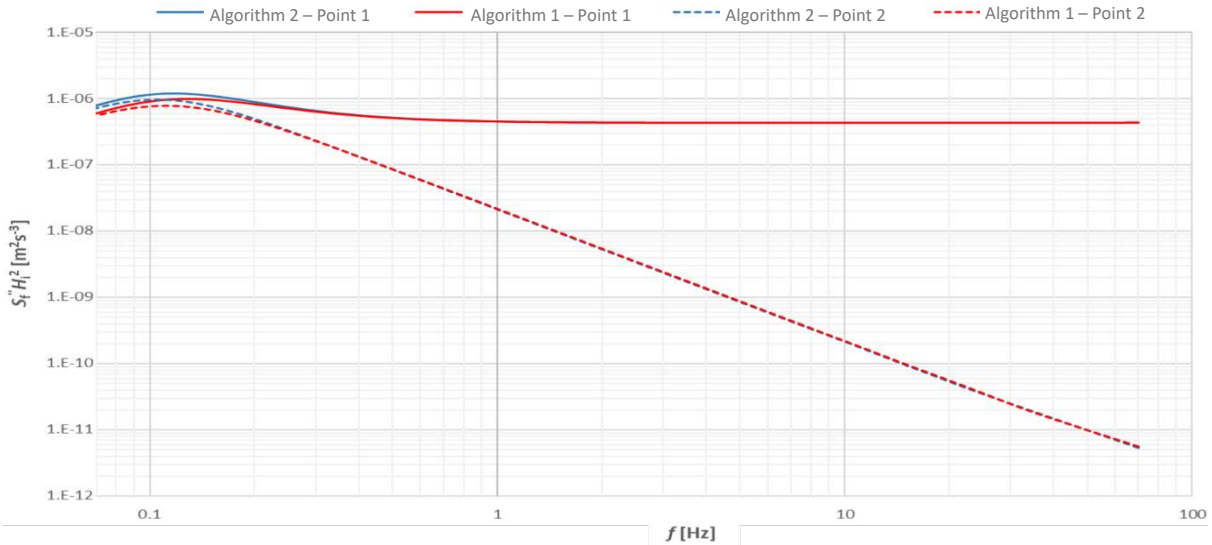

Figure 4.3: Acceleration density spectrum with v = 7 m s^{-1}.

order to improve passenger comfort.

Thus, without any additional attenuation measures, algorithm 2 offers a slightly better comfort than algorithm 1. The response can be further improved with the use of digital filters, namely in reducing the amplitude of the acceleration spectrum of point 1 in the high frequency range.

In figure 4.4 we can see the huge impact of digital filters in reducing the amplitude of the acceleration density spectrum of point 1 (front axle) for algorithm 2. For high frequencies (f > 10 Hz), the increase of the filter time step drastically reduces the amplitude; for a 1 s time step filter the reduction is around 5 orders of magnitude when compared to the case where no filter is applied. For lower frequencies, around 0,1 Hz, a increase in the filter time step leads to a amplification of the system response. The same happens for the algorithm 1 (see chapter 3.5 (Pereira, 2020))

Since the amplitude of the undesirable disturbances in this low frequency range is practically nil, this amplification is tolerable. A change in the radius of curvature is an example of a low frequency disturbance and in this case, an increase in the amplitude of the response may even be desirable. Above all, it is easy to control the low frequency (long wavelength) disturbances of the reflective tape, even compensating for the characteristics of the guiding system response.

Digital filters introduce a delay in the response that can impair guiding system, since when changing the trajectory we want a quick response from the vehicle. Thus, there is a need to evaluate the behavior of the system with digital filters in cases where the delay in the response may be an inconvenience. Let us examine the response of the guidance system to a step (see chapter 3.6 (Pereira, 2020)) and ramp disturbance (see chapter 3.7 (Pereira, 2020)).

Step Response

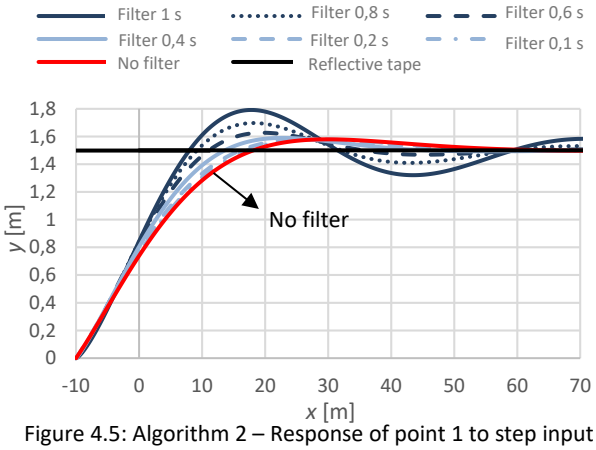

Figure 4.5: Algorithm 2 – Response of point 1 to step input

In figure 4.5, an increase in the time step of the digital filter causes an increases the overshoot and delays the response; however, it allows the vehicle to be closer to the desired position at x = 0 (longitudinal coordinate of the initial aiming point).

In chapter 3.6 (Pereira, 2020) we can observe that for the same filter, algorithm 2 has a slightly lower delay than algorithm 1. However, algorithm 1 has a smaller overshoot.

For both algorithms, the 0,6 s filter has a good compromise between the different parameters analyzed: it has a slightly longer establishment time when compared with the no filter response, but in the initial phase, brings the vehicle closer to the position of the reflective tape; at x = 0 about 16% closer in algorithm 1 and 12% in algorithm 2 (see figure 4.5),compared to response without digital filter). In addition, this filter drastically reduces the amplitude of the acceleration density spectrum of both algorithms for the critical guiding frequencies (f > 1 Hz - see figure 4.4).

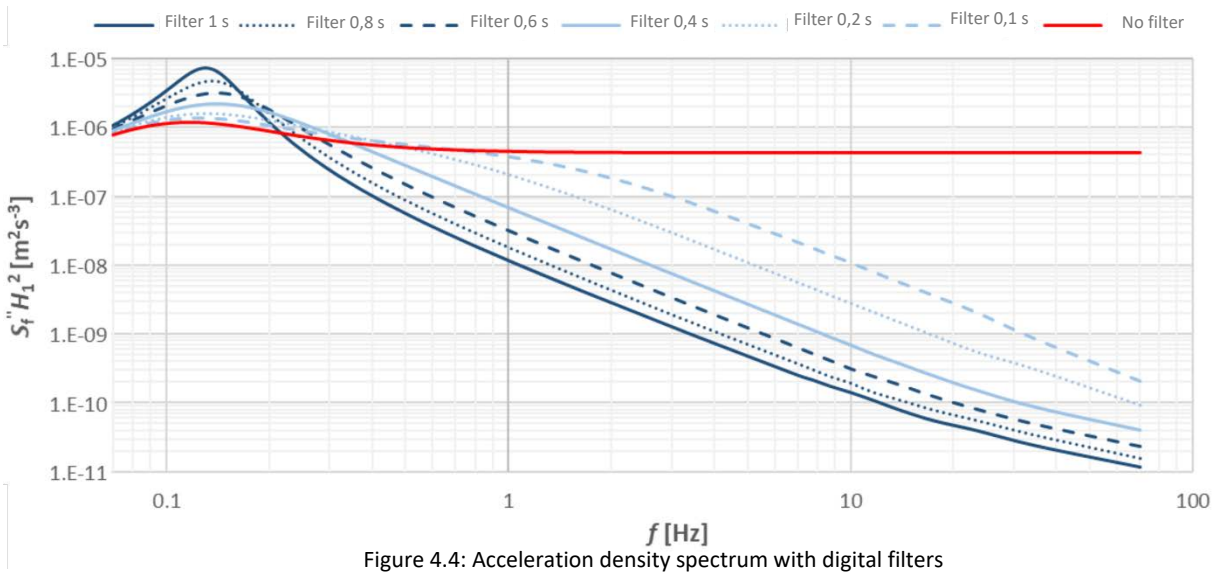

Figure 4.4: Acceleration density spectrum with digital filters for algorithm 2 with v = 7 m s^{-1}.

Ramp Response

Without any digital filters, both algorithms have a good response to the ramp input (for algorithm 2 see figure 4.6 and for algorithm 1 see chapter 3.7 (Pereira, 2020)), smoothing the sharp turn of the reflective tape without significantly deviating from it.

The application of digital filters slightly delays the response, but, in general, reduces the maximum deviation (which occurs at different places depending on the filter). It appears that a 1 s time step reduces the radius of curvature of the vehicle's trajectory, which impairs passenger comfort. As in the step response, the filter with a 0,6 s time step reduces the maximum deviation and provides a higher radius of curvature (better comfort). Either way, the differences in guiding system, with and without a filter, are small. For the tested example, the maximum deviation reaches only about 3 cm.

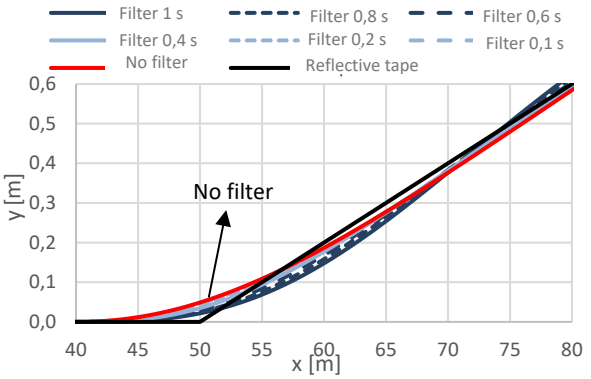

Figure 4.5: Algorithm 2 – Response of point 1 to ramp input

Errors in of local curvature radius database

The path taken by the vehicle is known, including the curvature radius of path.

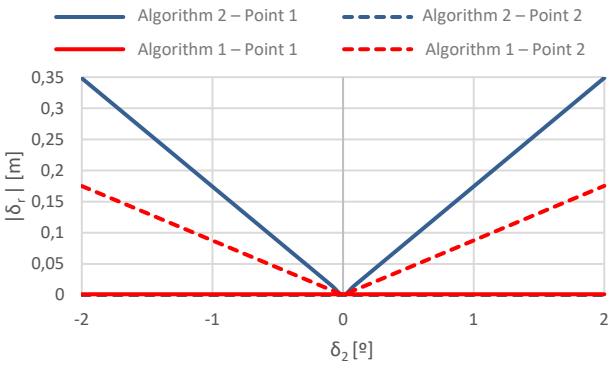

Figure 4.6: Lateral maximum deviation from errors in radius database.

Errors in database of these radiuses create a lateral deviation from the path to take that can affect the guiding system, thus, it is important to quantify the order of magnitude of this type of errors (for details see chapter 3.8 (Pereira, 2020)). They affect the angle θ_2 (see figure 4.1) since it is a function of the curvature radius R_s ($\sin\theta_2 = \frac{L_2}{2R_s}$). The disturbed rear axle angle can be given by $\widetilde{\theta_2} = \theta_2 + \delta\theta_2$ where θ_2 would be the correct angle if there was no error in the database and $\delta\theta_2$ is the angular deviation due to the errors in the database. In the tested examples, the error $\delta\theta_2$ is constant. The guiding system, based on the target point, corrects the angular deviation of the rear axle, but makes the vehicle describe a path radially deviated from the nominal curve.

Despite the way the two algorithms were designed, the axis that passes through the target point (point zero, see figure 4.1) has zero deviation. In algorithm 1, it is the front axle (point 1, see figure 4.1) that passes through the target point and in algorithm 2 it is the rear axle (point 2, see figure 4.1). This happens because the error in the mid angle of the rear axle (θ_2) is exactly compensated for the axle that must pass through point 0. Only the axes that "do not pass through the target point" suffer a deviation associated with the error induced in $\widetilde{\theta_2}$. This error is positive in algorithm 2 and negative in algorithm 1 .

Algorithm 2 has a maximum lateral deviation of δ_r = 35 cm for an error $\delta\theta_2 = \pm 2$ ° which, for a nominal radius of curvature of 50 m, means an error of ± 21 m in the database. For the same error, algorithm 1 has a maximum deviation of | δr | = 17 cm.

These deviations are small for such significant errors in the nominal radius of curvature, which demonstrates that both algorithms are robust for this range of errors (see figure 4.6). Therefore, in a transition between a straight line and a curve, the maximum deviations that would occur would be acceptable even if an error in the location of the vehicle induces an important error in the local radius of curvature.

Additionally, the transition between a straight line and a curve would never be abrupt, since there are concordance curves whose curvature varies smoothly and, therefore, is less sensitive to errors in longitudinal location, which would translate into smaller errors than those presented here and, therefore, the deviations would be smaller.

Image resolution errors

Every image taken by the video cameras has a resolution error associated with it. The order of magnitude of these errors needs to be estimated in order to evaluate its impact on the guiding system.

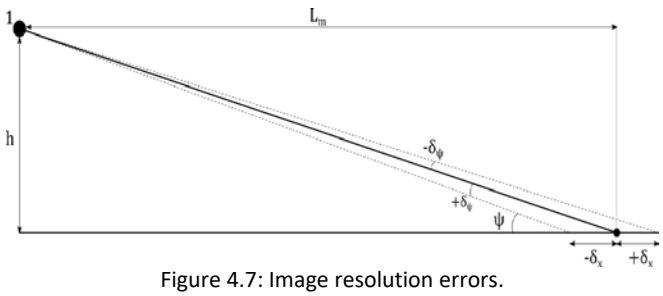

Figure 4.7: Image resolution errors.

Figure 4.7 shows the resolution errors associated with image recording of the reflective that guides the vehicle over its route. The uncertainty of each pixel correspond a certain angular uncertainty δ_ψ. The video cameras are

located at point 1 in front of the vehicle at height *h* from the ground. The longitudinal aiming length is $L_m = \sqrt{L_2^2 - h^2}$. The increments $\pm\delta_x$ represent the longitudinal errors due to image resolution. The aiming angle is $\tan\psi = \frac{h}{L_m}$. A HD720p camera has a 1280x720 pixels resolution. Let us consider that $L_2 = 10$ m and $h = 1{,}8$ m thus $L_m \sim 9{,}8$ m. If at this distance the frontal image area is 1,6 m x 0,9 m then $\delta_y = \delta_z = 1{,}25 \times 10^{-3}$ m in the vertical plane at 9,8 m with $\tan\delta_\psi = \frac{\delta_y}{L_m} = 1{,}27 \times 10^4$. Thus, the region recorded by the cameras in an orthogonal plane to the direction of the aiming is 1,57 m x 0,9 m. The uncertainty is $\delta_x = 2{,}25 \times 10^{-3}$ m in the lkongitudinal direction and $\delta_z = 1{,}25 \times 10^{-3}$ m in the transversal direction.

The video cameras have different bit depths that are used to define the colour of a pixel. An 8-bit bit depth means that there are 256 values that can be assigned to each of the colours of the RGB scale (red, green and blue) to define the tone of a pixel. Thus, an 8-bit camera allows 2563 different shades of colours to be represented.

Figure 4.8 shows the example of how pixels represent an edge of the reflective tape between the dark background on the left and the white band on the right. Pixels of greyish tones have a percentage of colour depending on the proportion of background or light band they catch. With this percentage and the pixel resolution, it is easy to obtain the distance from the edge of the ribbon (red line) to the edge of the pixel.

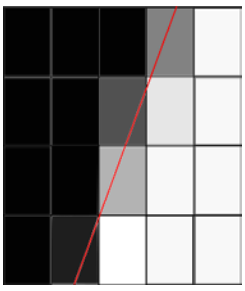

Figure 4.8: Pixel tonality over the edge of the reflective tape

The chromatic noise does not allow you to take advantage of the 256 shades of each color, but for each color on the RGB scale, you can reasonably distinguish about 10 shades of grey. Thus, the effective resolution of each colour is 1 order of magnitude smaller. Since the measurement of each of the three RGB colors is made independently, the average of uncertainty is even lower. Black and white colors are not always defined by the same bit on the RGB scale, there are slight variations along a row of pixels.

Figure 4.9 shows an example of a row of pixels and the bit that characterizes its color on the RGB scale. The dashed line represents the edge of the reflective tape. To calculate the distance from the edge of the tape to the edge of the pixel we can consider that the bit of the color 100% white is the average of the bits of the light zone and the color 100% black is the average of the bits of the dark zone for each of the three colors RGB. The white color is defined as R: 216, G: 214, B: 216 and the black color as R: 10, G: 9, B: 10. Therefore, for the red color, the edge of the ribbon is 35% distance from the edge of the dark area and 65% from the light area. If we now multiply this percentage by the effective resolution, we obtain that the edge of the tape is $7{,}9 \times 10^{-5}$ m from the dark area in the longitudinal direction. If we do the same for the other colors and consider the average of the three as the value, we have that the edge of the tape if it is $7{,}6 \times 10^{-5}$ m from the dark area.

In the scan it is confirmed that the differences between successive pixels are very small and then increase until it reduces again. The ribbon is in the middle, as shown in figure 4.8. The image processing can be intelligent and once the edge of the tape is determined in one iteration, in the next it is not necessary to scan the entire image, but rather an area close to the edge previously determined. Since the length of the tape is known, once one edge is determined, the other is also determined. This reduces the computing time and the need for processing capacity. In a specific target area, the tape position is measured in several rows in the longitudinal direction.

The measurements of this set of rows are an approximately normal distribution. For this type of distribution, the mean error is proportional to $\frac{1}{\sqrt{n}}$ where n is the sample size. This means that if we increase the number of points 100 times, the error decreases by a factor of 10. The sample size depends on the number of rows considered for the mean and the number of edges of each row. The sample size can be increased if the reflective tape consists of several parallel lines, each with two edges.

As a conclusion, the resolution error is smaller than the millimetre and thus, does not impact the guiding system.

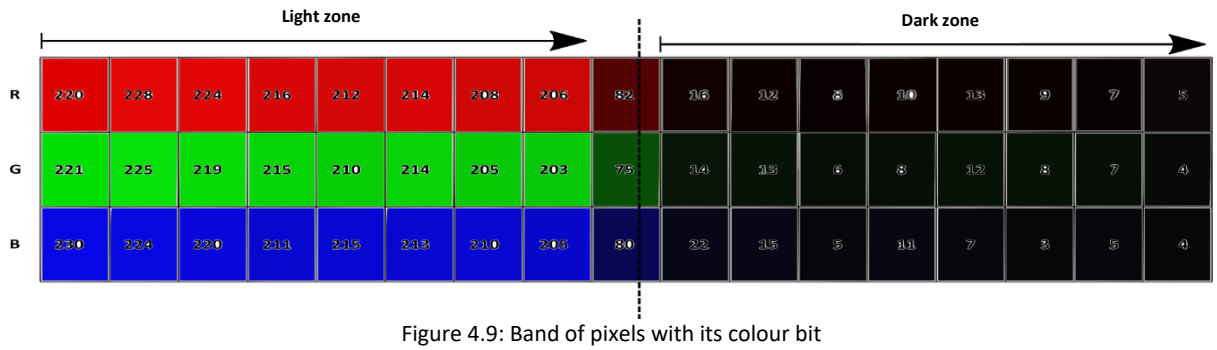

Figure 4.9: Band of pixels with its colour bit

5. Pre structural design

Another important aspect that is important to quantify is the tare weight of the vehicle. Structural design is very complex and requires a lot of considerations that are beyond our scope of work. In this thesis, the objective is to have a round estimate of the weight the vehicle and not a precise calculation.
In chapter 4 (Pereira, 2020) an approximated value for tare weight is computed. We compared the structure of the vehicle to a simply supported beam as shown in figure 5.1

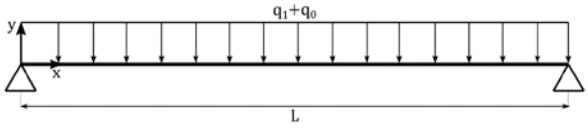

Figure 5.1: Simply supported beam

Furthermore, we considered the beam section to be a rectangular hollow section. We can use structural equations to estimate the weight of the beam taking into account some design criteria (see chapter 4.1 (Pereira, 2020)). We consider to different criteria: the maximum beam deflection $y_{max} \leq 1$ mm; maximum beam stress $\sigma_{max} \leq 100$ MPa. We observed that the limiting criterion was the maximum deflection and that 1 mm thickness would support a maximum vertical load q_1 of around 95 kN/m and weight around 280 kg if it were made of common steel. For this thickness and load the natural frequency of the structure would be around 78 Hz. That is a higher than the typical frequency ranges that affect vehicles structures. However, for a more detailed design we would need to inspect the local natural frequencies of the structure.

In chapter 4.1 (Pereira, 2020) we also computed the critical load that if surpassed would originate elastic instability, known as buckling. We saw that for frontal shock the critical load was around 10^4 times higher than the axial compression force that occurs. We also considered the case were the impact was with corner of the vehicle and once again the critical load was around 10^4 times higher than impact axial forces.

However, after the global design of the vehicle structure it is also important to estimate the weight of the reinforcements. One way to reinforce the vehicle is consider a structure made of sandwich panel because it increases the bending stiffness without the need of local reinforcements. The faces of the panel that are subject to traction/compression forces are made of high stiffness materials such as steel whereas the nucleus that transfers the transversal forces is made of low density material such as foam. Nevertheless, we considered an additional local reinforcement for the floor of the vehicle since it is subject to higher loads due the passenger's weight (see chapter 4.2 (Pereira, 2020) for details). We concluded that local reinforcement would weight around 360 kg. So considering the sandwich panel faces to have a 1 mm thickness and summing the local reinforcement for the floor, the total weight of vehicle would be around 920 kg. Comparing the vehicle to some commercial vans we see that this estimate is in the same order of magnitude, thus making this pre structural design a good approximation to get a round value for the vehicles weight. Considering the full vehicle with electric motors, batteries, tires and 10 passenger's and their luggage the total mass rises to 2200 kg and vehicle center of mass is 0,47 m above the steering axle.

6. Vertical dynamics: Two stage suspension

Vertical comfort is another crucial aspect of the vehicle design. A simple model to describe the vehicle response to vertical vibrations from the road unevenness is to consider ¼ of the vehicle strained to vertical motion, (fig x) with 2 DOF.

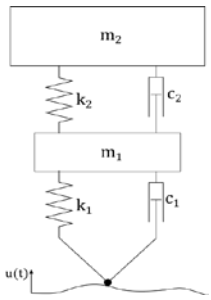

Figure 6.1: Two stage suspension model

The system of equations that control the vertical motion are (see chapter 5.1 (Pereira, 2020))

$$\begin{cases} m_2\frac{d^2y_2}{dt^2} + c_2\left(\frac{dy_2}{dt} - \frac{dy_1}{dt}\right) + k_2(y_2 - y_1) = 0 \\ m_1\frac{d^2y_1}{dt^2} + c_2\left(\frac{dy_1}{dt} - \frac{dy_2}{dt}\right) + k_2(y_1 - y_2) + c_1\left(\frac{dy_1}{dt} - \frac{du}{dt}\right) + k_1(y_1 - u) = 0 \end{cases},$$

The first stage represents the tire and the second stage represents ¼ of the vehicle's mass. For the calculations we considered a 15' tire with $k_1 \sim 282$ kN/m (this value already takes into account the road stiffness), $m_1 = 30$ kg (with the rim included) and a damping factor $\xi_1 = \frac{c_1}{2\sqrt{k_1 m_1}} \sim 0{,}01$ (see chapter 5.1 for a detail explanation).
Now, the objective is to see the effect of v ehicle's stiffness (k_2) and damping factor (ξ_2) on the vehicles response to the road unevenness. In chapter 5.1 (Pereira, 2020) we show the vehicle response for different values

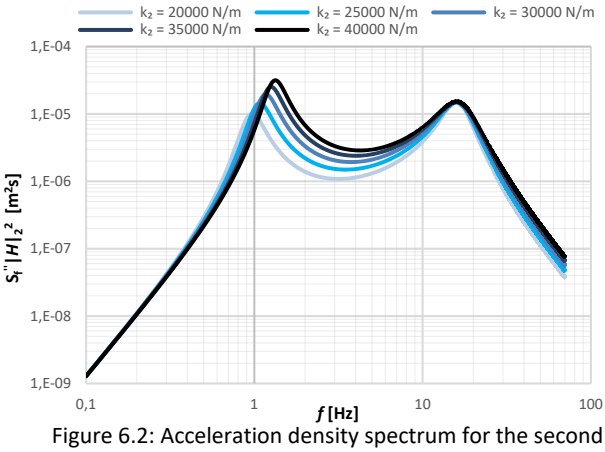

Figure 6.2: Acceleration density spectrum for the second stage of the suspension with $\xi_2 = 0{,}2$.

of k_2 and ξ_2. We consider class D/E of ISO 8608 to define the density spectrum of the vertical irregularities of the road.

In figure 6.2, we see that a smoother suspension results in lower resonance peaks in the first resonance and shifts its occurrence to lower frequencies. In addition, lower stiffness originates lower acceleration amplitudes for the frequency range more sensitive to humans. However, a problem that comes from reducing suspension stiffness is the increase in quasi-static deflections of the springs, which can cause instability in the vehicle. This deflection can take significant values in acceleration/deceleration situations, causing an inclination in the suspension axle, which, in the case of acceleration, raises the front of the vehicle, decompressing the front suspension springs and lowering the rear by compressing the rear suspension springs. In the case of deceleration, the opposite occurs. For a vehicle with 2 ton vehicle with center of mass at 0,47 m above the steering axle the deflections are in order 1 cm for k_2 = 20 kN/m, a value that does not compromise the vehicle stability.

Ramp Response

In figure 6.3 we can see that the more rigid the suspension is, the smaller the deviation between the ramp and the vehicle's response. The oscillation time is also shorter, reaching the equilibrium position more quickly (see chapter 5.2 (Pereira, 2020))

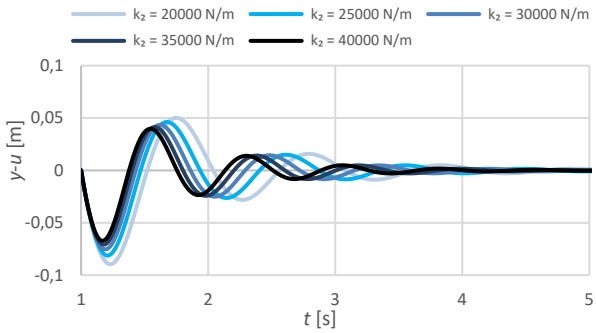

Figure 6.3: Vehicle's deviation to a 5% inclination ramp input with ξ_2 = 0,2.

Bump Response

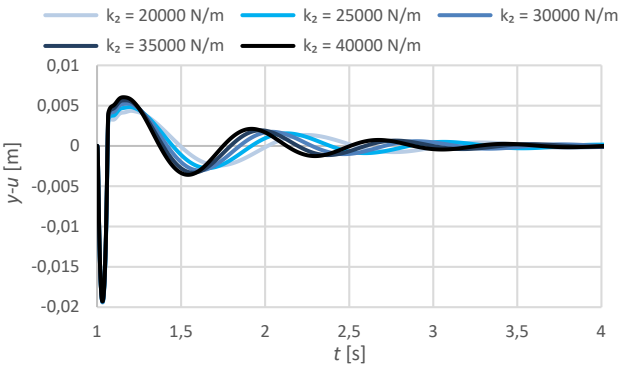

Figure 6.4: Vehicle's deviation to bump input with a height of 2 cm, 0,5 m length and ξ_2 = 0,2.

In figure 6.4 we can see that for a constant damping factor an increase in suspension stiffness increases the amplitude of vehicle's response, however, it decreases the oscillation time reaching thee equilibrium position earlier (see chapter 5.3 (Pereira, 2020)). A stiffness of 20 kN / m and a damping factor of 0.2 for the second stage of the suspension allow a good response both for ramp and for bump and reduces the amplitude of acceleration spectrum in the critical frequency range.

7. Conclusion

The main objectives define for this thesis were achieved. We were able to make to design a cheap, reliable and comfortable autonomous vehicle cable of transporting passengers from airport terminals to airplanes.

A nominal velocity of 7 m s^{-1} allows small travelling times a larger fleet productivity without compromising the development of cheap and reliable guiding system. A traction power of 4 kW, divided into 1 kW electric motors for each wheel (costing 150€/each) is enough to reach the nominal speed and allows the vehicle to climb to the first floor of terminals, making a typical trip in around 3,5 min when it full with passengers with average energy consumption of 181 Wh/km. A total of 85 kg of lithium batteries (costing 4.1 k€) are enough to allow 10 h of continuous operation

The guiding system presented is a simple and easy to implement, based on a set of video cameras and a digital image processing method. Without filters, the algorithms are relatively robust and the vehicle has maximum lateral deviations of the order of 30 cm for the worst cases. The introduction of a digital filter substantially reduces optical noise and drastically reduces the amplitude of the acceleration spectrum by about 5 orders of magnitude, thus offering better comfort for passengers. Analyzing the response to disturbances of the step and ramp type, there was also an improvement in the guidance response when a filter was applied, reducing overshoot and maximum deviations.

In the pre structural design the vehicle mass was estimated to be around 920 kg and when full loaded around 2200 kg, thus having a center of mass at 0,47 m above the steering axle.

The vehicle suspension is similar to that of vehicles of similar size. A damping factor of ξ_2 = 0,2 and a stiffness of k_2 = 20 kN / m for the second stage of the suspension allow a good response both for ramp and for bump input. Also reduces the acceleration spectrum by about an order of magnitude when compared to more rigid suspensions, which would be necessary if this vehicle had to travel on uneven terrain.

References

André , J. M. C., Pereira, I. & Miranda dos Reis, V., 2017. *Expansão da capacidade do aeroporto de Lisboa: acesso eficiente e direto às posições remotas,* Lisboa: s.n.

André, J. M. C. S., 2006. *Transporte interurbano em Portugal: Concepção técnica de uma alternativa ferroviária para o transporte de passageiros.* Lisboa: IST Press.

Pereira, G. d. S., 2020. *Dimensionamento de uma frota de veículos.* Lisbon: s.n.